

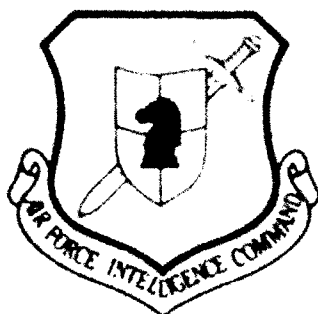
AD-A263 100



FASIS ID:K511-0311-92

2

# FOREIGN AEROSPACE SCIENCE AND TECHNOLOGY CENTER

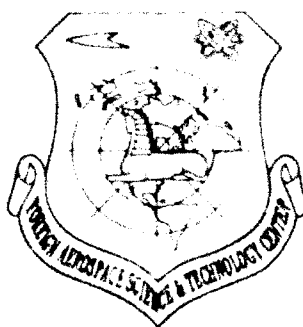


THE INFRARED MEASUREMENT FOR THE REENTRY-BODY

by

Zhao Gongzhong

DTIC  
APR 14 1993  
S B D



Approved for public release;  
Distribution unlimited.



93-07714



13478

93 4 18 052

# HUMAN TRANSLATION

FASTC-ID(RS)T-0311-92

2 April 1993

MICROFICHE NR: 93000243

THE INFRARED MEASUREMENT FOR THE REENTRY-BODY

By: Zhao Congzhong

English pages: 9

Source: Hongwai Yaniju, Vol. 7, Nr. 3, 1988;  
pp. 219-223

Country of origin: China

Translated by: SCITRAN

F33657-84-D-0165

Requester: FASTC/TATV/Capt J. Michael Phillips

Approved for public release; Distribution unlimited.

Accession For	
NTIS GRA&I	<input checked="" type="checkbox"/>
DTIC TAB	<input type="checkbox"/>
Unannounced	<input type="checkbox"/>
Justification	<input type="checkbox"/>
By	
Dissemination	<input type="checkbox"/>
Approval Agency	
Approval	
Dist	<input type="checkbox"/>
A-1	

THIS TRANSLATION IS A RENDITION OF THE ORIGINAL FOREIGN TEXT WITHOUT ANY ANALYTICAL OR EDITORIAL COMMENT STATEMENTS OR THEORIES ADVOCATED OR IMPLIED ARE THOSE OF THE SOURCE AND DO NOT NECESSARILY REFLECT THE POSITION OR OPINION OF THE FOREIGN AEROSPACE SCIENCE AND TECHNOLOGY CENTER.

PREPARED BY

TRANSLATION DIVISION  
FOREIGN AEROSPACE SCIENCE AND  
TECHNOLOGY CENTER  
WPAFB, OHIO

#### GRAPHICS DISCLAIMER

All figures, graphics, tables, equations, etc. merged into this translation were extracted from the best quality copy available.

FASTC - ID(RS) T - 0311 - 92

The Infrared Measurement for the Reentry-Body

Zhao Congzhong

(207 Research Institute, Ministry of Astronautics Industry)

Translation from Hongwai Yanjiu (Chinese Journal of Infrared Research), Vol. 7A, No. 3, June 1988

Translated by:

S C I T R A N

1482 East Valley Road

Santa Barbara, CA 93150

# The Infrared Measurement for the Reentry-Body

Zhao Congzhong

(Ministry of Astronautics Industry)

(Received Aug. 10, 1987)

**Abstract:** The measured results of a reentry-body by a PbS radiometer are described in this paper. The standoff range of the radiometer reaches 100 km. Some features about the target are given.

## I. Introduction

When any space reentry-body enters the atmosphere of the earth at super fast speed, violent photo electric synthesis phenomenon occurs immediately. Surrounding the reentry-body is a high temperature plasma sheath, which severely disrupts and even stops the radio signals used for remote measurement. In the mean time, large amount of hot ultraviolet, visible and infrared signals are radiated. Exploration and utilization of the series of radiated light signal caused by the spaceship reentering the atmosphere can help to provide precision guidance, and to predict the return target of the spaceship<sup>[1,2]</sup>.

## II. Basis Principle

When a super fast reentry body enters the atmosphere, due to the extremely high temperature caused by the violent aerodynamic heating, the highest wall temperature can reach 3000~4000K (the temperature at the stagnation point reaches 8000K); the wake has a length of 880m; tremendous power of ultraviolet, visible and infrared energy is radiated.

The light radiation power can be described by the rate of change of the kinetic energy<sup>[3]</sup>:

$$\frac{d(KE)}{dt} = \frac{1}{2} v^2 \frac{dm}{dt} + m v \frac{dv}{dt}, \quad (1)$$

where,  $V$  is the speed of the reentry body,  $\frac{dV}{dt}$  the acceleration of the reentry body,  $m$  the mass of the reentry body,  $\frac{dm}{dt}$  the burning rate of the protective material.  $V$  and  $\frac{dV}{dt}$  are measured by radar and projectile camera.  $m$  is a known quantity. Once the material is selected,  $\frac{dm}{dt}$  is determined by burning experiments of the material in ground based plasma arc wind tunnel.  $\frac{d(KE)}{dt}$  can be calculated from formula (1). Formula (1) can be used for the reverse design and prediction of the light radiation efficient of planned reentry body.

/220

In addition, the radiation power can also be obtained from the following formula and using optical measurement to check the result.

$$W_{\lambda} = \frac{4\pi R^2 H_{\lambda}}{T_{a\lambda}} \quad (2)$$

where

$$H_{\lambda} = V_s / V_N \cdot NEFD, \quad (3)$$

and

$$J = \frac{R^2 H_{\lambda}}{T_{a\lambda}}. \quad (4)$$

Among the above formulae,  $R$  is the curvilinear distance between the reentry body and the radiometer,  $H_{\lambda}$  the degree of radiation at the reception hole of the radiometer ( $W/cm^2$ ),  $T_{a\lambda}$  the atmospheric penetration rate between the reentry body and the radiometer,  $V_s$  the voltage signal (mV) measured by the radiometer of the reentry body,  $V_N$  the sky background voltage signal ( $\mu V$ ) measured by the radiometer,  $NEFD$  the system sensitivity of the radiometer ( $W/cm^2$ ),  $J$  the radiation strength of the reentry body ( $W/Sr$ ).

### III. Measuring equipment and calibration

The measuring equipment consists of an optical probe and electronic data processors. The optical probe consists of main mirror (1), secondary mirror (2), motor (3), modulation disk (4), light cone (5), and PbS component (6). The electronic data

processors consist of preamplifier, 2107 spectrum analyzer, 2305 recorder, and a timer as shown in Fig. 1.

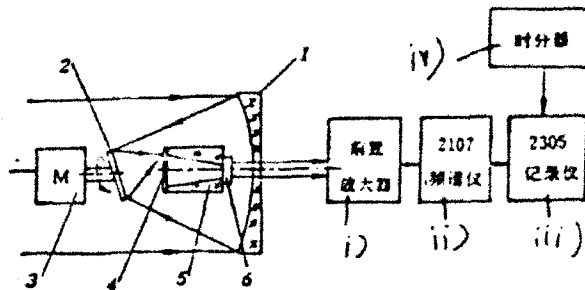


Fig. 1 Schematic diagram of the radiometer. i) Preamplifier, ii) spectrum analyzer, iii) recorder, iv) timer.

### 1. Optical probe

This system uses the Newton's system. The main mirror is a parabolic mirror with diameter  $D = 250\text{mm}$ . The secondary mirror is a planar mirror with diameter  $d = 110\text{mm}$  and focus  $f = 680\text{mm}$ . The view angle of the system is  $2\omega = 3^\circ 7'$ . The component is PbS with dimension  $6 \times 6\text{mm}$ . The wave band is  $1\sim 3\ \mu\text{m}$ . The working temperature is the room temperature.  $D^* = 0.5\sim 2 \times 10^9\ \text{cmHz}^{1/2}/\text{W}$ . It has a germanium window. The aperture entry diameter of the light cone is  $\phi = 20\text{mm}$ , the exit diameter  $\phi = 5\text{mm}$ . It has strip slit whose gap is 1 mm and parallel to the reentry direction. The linear region of the modulation disk is  $20\sim 24'$ . The secondary mirror is driven by the motor to form a small angle with the perpendicular line of the light axis so that the incident light does conic scan and the scanning circle falls on the focusing surface (i.e. on the modulation disk); the size of the trace of the scanning circle is  $\phi = 10\text{mm}$ . The frequency of the signal is determined by the product of the rotation rate of the motor and the number of the slits on the modulation disk. The low frequency background cloud is filtered by frequency selection in order to enhance the useful signal of high frequency target. The size of the dispersion circle of the optical system is  $0.3\text{mm}$ .

### 2. Electronic system

The lead of the PbS component is connected to the preamplifier with a magnification of 10. Since this type of strip

modulation disk is rich in modulating signal frequency, the 2107 spectrum analyzer is used for frequency selection and the result is tape recorded by the 2305 recorder. The real frequency selection is 500 Hz. The timer supplies one time mark in one second and prints it on the recording paper. The selected paper speed is 1 cm/s. The specifications of the preamplifier are:  $f=1$  kHz, magnification 10, the maximum output power 220mV, input impedance  $2.8M\Omega$ ; the open circuit noise is  $10\mu V$ , and when component is connected ( $510k\Omega$ ) it is  $5.6\mu V$ ; the bandwidth is 30-80kHz; the linear range of the voltage input is 2-200mV and hence the linear range of the output voltage is 20-2000mV.

### 3. Instrument calibration

#### (1) Calibration equipment

The calibration system is shown in Fig. 2. Site calibration can be carried out during a dark night.

1221

It should be pointed out that radiometer calibration must be conducted under the condition of alignment infrared radiation source proposed in Ref [4]. Here, according to the practical conditions, the radiometer is calibrated by placing it at a distance of 166m from the black-body stove. The opening angle of the black body with respect to the radiometer is very small so that the alignment is guaranteed and the relative error is not greater than 1%. Calibration is done before and after the test to prevent the variation of the radiometer sensitivity due to some unforeseen factors. Calibration is done for the full range and the full linear scope.

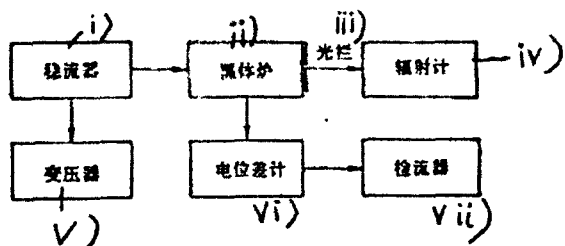


Fig. 2 The calibration system. i) current stabilizer, ii) black-body stove, iii) diaphragm, iv) radiometer, v) transformer, vi) potentiometer, vii) current detector.



## (2) Calibration result

The sensitivity formula of the radiometer system is

$$NEFD = \frac{\epsilon \sigma T^4 \Delta S \tau}{L_0^2 \pi V_S / V_N} \quad (5)$$

where  $\epsilon$  is the emission coefficient,  $\sigma$  the Stephen-Boltzman constant,  $T$  the temperature (K) of the black-body stove,  $\Delta S$  the surface of radiation of the black-body stove,  $\tau$  the atmospheric permeability between the black-body stove and the radiometer,  $L_0$  the distance between the black-body stove and the radiometer[4]. When the calibration condition is taken from the infrared radiation which is obtained by placing the black-body stove at the focal length of a single reflector aligner,  $L_0=f_0$  in formula (5).  $V_S$  is the black-body voltage signal of the black-body stove measured by the radiometer.  $V_N$  is the background noise of the black-body stove. If the various parameter values measured from the site calibration condition ( $T=838.8K$ , the radiation hole diameter of the black-body stove  $\phi=1.5cm$ ,  $L_0=166m$ ,  $V_S=15.5mV$ ,  $V_N=165\mu V$ ,  $\tau=0.4$  etc.) are substituted into formula (5), it follows that  $NEFD=4.48 \times 10^{-12} W/cm^2$ .

## IV. Measurement results

### 1. Main measurement results

The observable time of the site reentry phenomena is about 25s. The processed actual data are shown in Table 1.

Table 1 The radiant measurement values for the reentry-body.  
i) reentry parameters, ii) measured values of the light radiation.

i) — 再 入 参 数			光 辐 射 测 量 值 — ii)			
$t(s)$	$h(km)$	$R(km)$	$V_s(mV)$	$V_S/V_N$	$H(W/cm^2)$	$J(W/Sr)$
0	54.3	97.2	48	192	$8.6 \times 10^{-10}$	$4.1 \times 10^5$
3	46.5	85.4	593	2371	$10.6 \times 10^{-9}$	$3.7 \times 10^6$
6	38.6	72.6	1000	4000	$1.8 \times 10^{-8}$	$4.7 \times 10^6$
9	30.7	58.9	1117	4466	$2.0 \times 10^{-8}$	$3.4 \times 10^6$
12	22.9	46.1	548	2192	$9.8 \times 10^{-9}$	$1.1 \times 10^6$
15	15.3	34	531	2125	$9.5 \times 10^{-9}$	$5.4 \times 10^5$
18	8.7	24.5	803	3214	$1.4 \times 10^{-8}$	$4.2 \times 10^5$
21	3.2	17.6	71	286	$3.8 \times 10^{-10}$	$2.0 \times 10^4$

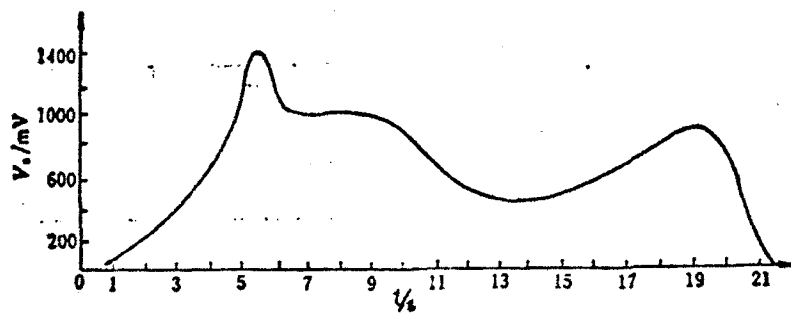
In the table,  $t$ ,  $h$ , and  $R$  are the time, the height of the reentry body, and the curvilinear distance respectively.  $V_N$  is the background noise of the sky; the site measured value is  $V_N=250\mu V$ . The weather was good during the measurement and the measured values of the background are consistent.

## 2. Reentry radiation curve

(1) The curve  $V_s=f(t)$ , describing the relationship between the reentry radiation voltage signal and the time change, is shown in Fig. 3.

Fig. 3 indicates that the variation of the signal is affected by the rolling characteristics of the target, the changes of the lighting angles of the sun on the target, the reflection properties of the earth, the instrument alignment precision, the target mass resistance ratio, the atmospheric transport, and the dispersion properties. The curve shows that, in general, the reentry radiation signal changes from small to large and then from large to small. It reaches the maximum at the height of 40 km and causes the instrument data indicator to reach the saturation values. The range of variation is as high as  $10^3$ . The maximum radiation power is  $W_\lambda \approx 5 \times 10^7 W$ .

/222



(2) The curve  $J=f(h)$ , indicating the reentry radiation strength variation as a function of the height, is shown in Fig. 4. The maximum radiation strength reached at the height of 40km is  $J \approx 4 \times 10^6 W/Sr$ .

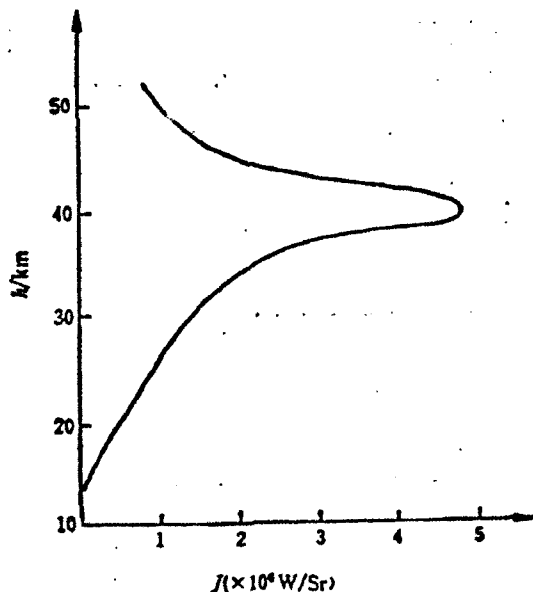
### 3. Simple analysis

(1) When the reentry speed increases to approximately 4.5km/s (the corresponding height is approximately 40km), deceleration phenomenon starts to occur, manifested by the strong and violent aerodynamic heating drag effect which lasts until the falling when the speed is reduced to about 2.4km/s.

(2) Both the sudden change of the speed of the reentry phenomenon and the corresponding sudden change of the light radiation occur at the height of approximately 40km, which is basically consistent with the sudden increase of the radar echo measurement. The wake has an obvious reaction.

(3) The measured reentry body radiation power is about  $10^4 \sim 10^8$  W. The radiation strength is  $J = 10^3 \sim 10^7$  W/Sr. It is reported that a body of weight 900kg with reentry velocity 6km/s and acceleration of 50g can generate  $3 \times 10^9$  W total radiation power. This can be compared with our measured values. Thus it shows that super fast reentry body is a very strong source of visible and infrared radiation. It is similar to a third grade star during the night and is 1000 brighter than the planets.

(4) Even with the complexity of the site test conditions, our data have shown that, under good weather condition, for a 4.5km/s reentry body, the light radiation signal of a reentry body target at 100km curvilinear distance can be received completely by PbS radiometer.



## V. Summary

1. The test shows the success of measuring far away super fast reentry body light radiation characteristics by our PBS radiometer. The curve shape of the measured values reflects the reentry properties and the laws very faithfully.

2. The measured maximum signal to noise ratio is  $V_S/V_N=4466$  corresponding to the height of 31km. When at the farthest curvilinear distance of 97.2 km, the signal to noise ratio is  $V_S/V_N=192$ . These is still potential to extend the range of the radiometer.

/223

3. Due to the complexity of the test environment, the test equipment, measuring method, and the measuring precision need to be further perfected and improved.

**Acknowledgment:** We express our thanks to Mr. Xu Gengxin for organizing the system engineering of the reentry measurement and to Mr. Yao Lianxin for precious suggestions.

## Reference

- [1] Ried R. C. Jr. et al, NASA TMX-58091, April 1972, 2.
- [2] Cecil Brownlow, Aviation Week July 14, 1958, 33.
- [3] Robert V. Meyer, Applied optics January, 5(1966), 1; 159.
- [4] Richard D. Hudson Jr., Infrared System Engineering, 1969, 225.

# DISTRIBUTION LIST

## DISTRIBUTION DIRECT TO RECIPIENT

ORGANIZATION	MICROFICHE
B085 DIA/RIS-2FI	1
C509 BALLOC509 BALLISTIC RES LAB	1
C510 R&T LABS/AVEADCOM	1
C513 ARRADCOM	1
C535 AVRADCOM/TSARCOM	1
C539 TRASANA	1
Q592 FSTC	4
Q619 MSIC REDSTONE	1
Q008 NTIC	1
Q043 AFMIC-IS	1
E051 HQ USAF/INET	1
E404 AEDC/DOF	1
E408 AFWL	1
E410 ASDTC/IN	1
E411 ASD/FTD/TTIA	1
E429 SD/IND	1
P005 DOE/ISA/DDI	1
P050 CIA/OCR/ADD/SD	2
1051 AFIT/LDE	1
PO90 NSA/CDB	1
2206 FSL	1

Microfiche Nbr: FTD93C000243  
 FTD-ID(RS)T-0311-92